ISSN 1070-4272, Russian Journal of Applied Chemistry, 2020, Vol. 93, No. 10, pp. 1615–1627. © Pleiades Publishing, Ltd., 2020.

CATALYSIS

Fabrication of Highly Active Ag_3PO_4/ZnO/Diatomite for Visible Light Photocatalytic Degradation of Tetracycline Hydrochloride

Pengfei Zhu[a,b,*], Ming Duan, Ruoxu Wang[a], Hao Lei[a], Min Hu[a], Mei Liu[a], Xiaoluo Cheng[a], and Baofu Li[a]

[a] *School of Chemistry and Chemical Engineering, Southwest Petroleum University, Chengdu, 610500 China*

[b] *Research Institute of Industrial Hazardous Waste Disposal and Resource Utilization, Southwest Petroleum University, Chengdu, Sichuan, 610500 China*

**e-mail: swpua124@126.com*

Received May 17, 2019; revised July 31, 2020; accepted August 2, 2020

Abstract—A novel Ag_3PO_4/ZnO/diatomite composite photocatalyst was prepared by simple ultrasonic dispersion-precipitation method. The structure, composition, microstructure and optical properties of the catalysts were characterized by means of X-ray diffraction (XRD), fourier transform infrared (FT-IR), X-ray photoelectron spectroscopy (XPS), scanning electron microscopy (SEM), energy dispersive spectrometer (EDS), transmission electron microscope (TEM) and UV-vis diffuse reflectance spectra (UV-vis DRS). Moreover, the visible light catalytic performance of the catalyst was investigated with tetracycline hydrochloride (TC) as the degradation target. The results showed that the photocatalytic activity of Ag_3PO_4/ZnO/diatomite in the degradation of TC, which can reach 90.99% removal rate of 30 mg/L TC under visible light, was significantly better than that of monomer catalysts and Ag_3PO_4/ZnO catalyst. Meanwhile, it exhibited better stability compared with pure Ag_3PO_4. The improvement of visible light catalytic activity and stability of Ag_3PO_4/ZnO/diatomite is mainly attributed to the catalyst's better adsorption capacity, wider spectral response range, more efficient photo-generated electrons and holes migration and less photocorrosion. The results of free radical trapping experiments show that the main active species of the reaction system are h^+ and $\bullet O_2^-$.

Keywords: Ag_3PO_4/ZnO/diatomite, visible light-responsive, photocatalytic degradation, tetracycline hydrochloride

DOI: 10.1134/S107042722010171

INTRODUCTION

Antibiotics are widely used in the medical industry, aquaculture, animal husbandry and other industries due to their good antibacterial and bactericidal effects [1]. But while antibiotics bring great convenience to human society, they are also regarded as "universal drugs" and "animal health products", which have reached the level of abuse [2]. After being absorbed and metabolized by humans and animals, antibiotics usually enter the water environment in the form of original drugs and metabolites. The residue of antibiotics in the water body will increase the resistance of pathogenic microorganisms, and even cause the "three effects (mutagenesis, carcinogenesis and teratogenesis)", causing huge harm to the ecological environment and human health [2–4]. Therefore, the treatment of antibiotic wastewater is imminent. At present, the main methods of treating antibiotic wastewater are adsorption [5], microfiltration combined reverse osmosis [6], ozonation [7] and photocatalytic oxidation [8–10]. Among them, the photocatalyst oxidation, whose device is simple, operation is easy, energy consumption is low, has effective degradation to pollutants without secondary pollution. It has become a research hotspot in this field. The key to this technology is to develop a photocatalyst which has high visible light activity and stable performance [9, 10]. As a new type of photocatalyst with good visible light responsiveness,

Ag_3PO_4 shows great potential in degrading organic pollutants such as dyes and antibiotics [11, 12]. However, Ag_3PO_4 is slightly soluble in aqueous solution, prone to photocorrosion, easy recombination of photogenerated electrons and holes, poor stability, and high cost, which limits its practical application to a certain extent [13]. Studies have shown that the formation of heterojunctions by selecting semiconductors with appropriate energy band structures and Ag_3PO_4 is one of the most effective ways to promote the separation of photogenerated electrons and holes of Ag_3PO_4, inhibit Ag_3PO_4 photocorrosion, and improve the activity and stability of Ag_3PO_4-based photocatalysts [14-20]. As a traditional semiconductor photocatalytic material, ZnO has become the most commonly used photocatalyst due to its advantages such as strong oxidation ability, stable chemical properties, low cost, non-toxicity, and environmental friendliness. However, ZnO has a wide band gap and can only be excited by ultraviolet light, and photogenerated electrons and holes are easily recombined, which go against its practical application [21–25]. Studies have shown that the conduction band (CB) and valence band (VB) potentials of ZnO are about –0.5 and 2.7 eV, and the CB and VB potentials of Ag_3PO_4 are about 0.45 and 2.9 eV. The energy bands of the two are highly matched, and they can be combined to construct a heterojunction catalyst. In the composite catalyst, ZnO can be used as a catalyst substrate to promote the transfer of electrons in Ag_3PO_4, which can effectively prevent the photocorrosion of Ag_3PO_4 and enhance its stability; on the other hand, Ag_3PO_4 as a photosensitive material has more negative valence band position can absorb visible light and greatly enhance the visible light catalytic activity of the catalyst [26, 27]. In addition, after the photocatalytic reaction is completed, it is difficult to separate the suspended Ag_3PO_4 powder from the solution, which affects its recycling, and the high cost of Ag_3PO_4 also affects its application. Research shows that the loading of Ag_3PO_4 on molecular sieve [28], SiO_2 [29], hydroxyapatite [30], palygorskite [31], bentonite [10, 32], attapulgite [33], diatomite [34] and other carriers with excellent adsorption performance can not only solve the above problems, but also further improve its photocatalytic efficiency.

In order to take advantage of the synergistic effect of Ag_3PO_4 and ZnO, improve the photocatalytic performance and reuse stability of the catalyst, this paper combines the narrow band gap Ag_3PO_4 and the wide band gap ZnO semiconductor by ultrasonic dispersion-precipitation method to construct heterojunction catalyst. The natural adsorption material diatomite, which is rich in resources, low in price, large in specific surface area, good in adsorption performance and stable in nature, is used as a photocatalyst carrier, and Ag_3PO_4 and ZnO are immobilized to prepare Ag_3PO_4/ZnO/diatomite ternary composite photocatalyst, then, the sample's phase composition, structure, morphology and optical properties were analyzed. By taking tetracycline hydrochloride (TC) as the degradation target, the visible light catalytic activity and cycle stability of the photocatalyst were investigated. Combined with the detection results of photocatalytic active species, the mechanism visible light catalytic degradation of TC by Ag_3PO_4/ZnO/diatomite was proposed.

EXPERIMENTAL

Preparation of ZnO

A certain amount of $Zn(NO_3)_2 \cdot 6H_2O$ and polyvinylpyrrolidone (PVP) was weighed into a beaker, and stirred well to dissolve in 50 mL pure water with ultrasonically dispersing for 5 min. Under stirring conditions, a certain volume of NaOH (0.2 M) solution was added dropwise according to the metering ratio. After the addition was completed, stirring was continued for 30 min in a constant temperature water bath at 40°C. Then cooling to room temperature, the precipitate was washed with pure water and absolute ethanol and centrifuged, and was vacuum dried at 60°C for 6 h, and at last, was calcined at 500°C for 2 h to prepare zinc oxide.

Preparation of Ag_3PO_4/ZnO/Diatomite

Ag_3PO_4/ZnO/diatomite composite photocatalyst was prepared by ultrasonic dispersion-precipitation method. 50 mL pure water were added in a beaker, then ZnO (0.186 g) was added with ultrasonically dispersing for 30 min. Then $AgNO_3$ (1.510 g) was added before continuously ultrasonic dispersing for 30 min. After that, a certain volume of Na_2HPO_4 solution (0.04 M) was added until the yellow precipitate of silver phosphate is completely precipitated, and at last, 0.500 g of diatomite was added and dispersed by ultrasonic for 30 min. Then the precipitate was washed 3 times with pure water and absolute ethanol. The washed precipitate was placed in a vacuum drying oven at 60°C and dried for 6 h. After

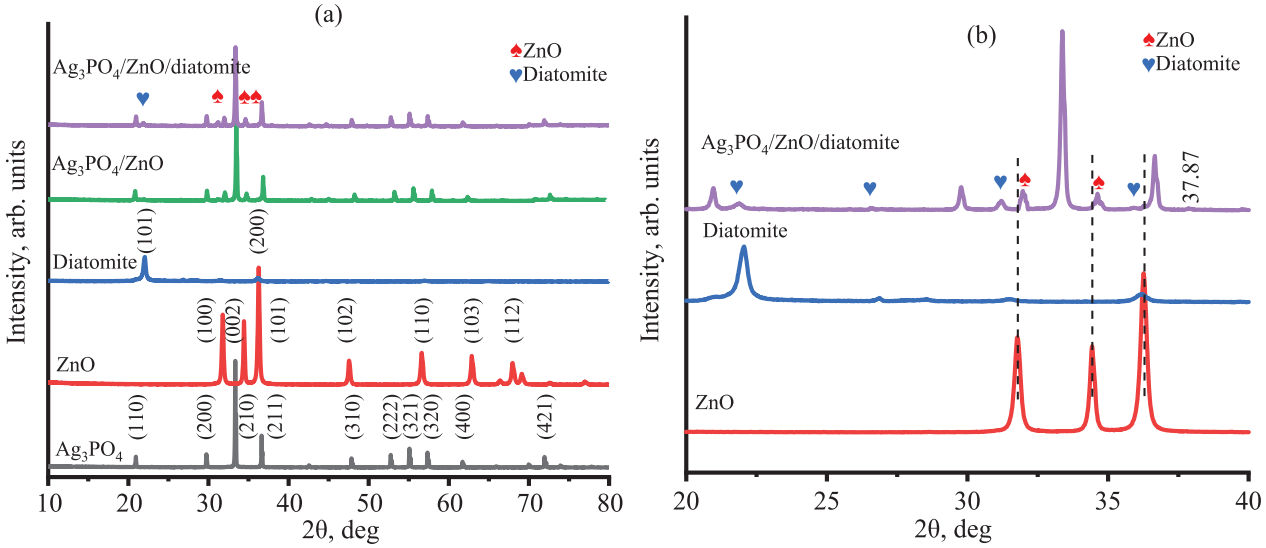

Fig. 1. (Color online) XRD patterns of (a) Ag_3PO_4, ZnO, diatomite, Ag_3PO_4/ZnO and Ag_3PO_4/ZnO/diatomite; (b) partial enlarged view of ZnO, diatomite, Ag_3PO_4/ZnO/diatomite.

cooling, it was ground evenly to prepare an Ag_3PO_4/ZnO/diatomite photocatalyst, which was stored in the dark. In the Ag_3PO_4/ZnO/diatomite composite photocatalyst, m(ZnO) : m(Ag_3PO_4) = 15 wt %, m(diatomite) : m(ZnO + Ag_3PO_4) = 35 wt %. According to the same method, Ag_3PO_4/ZnO and pure Ag_3PO_4 photocatalyst can be prepared, respectively.

Characterization of the As-Prepared Photocatalysts

XRD patterns of the samples were recorded on an X-ray diffractometer (PANalytical B.V., X'Pert Pro MPD) by using nickel-filtered CuK_α radiation (λ =1.54060 Å) in the range of $5° \le 2\theta \le 80°$.

FT-IR spectra were obtained on WQF-520 spectrometer using KBr as the beam splitter.

XPS were performed on a Thermo Scientific K-Alpha X-ray photoelectron spectrometer with an Al-K_α radiation.

The morphology and microstructure of the samples were investigated by a SEM (JEOL, JSM-7500F). The elemental compositions and distributions were analyzed by EDS.

TEM images were observed by a FEI Tecnai F20 field emission transmission electron microscope.

The UV-vis diffuse reflectance spectra (UV-vis DRS) were conducted on a UV-vis spectrophotometer (UV-1800, Shimadzu, Japan) using $BaSO_4$ as a reference.

Photocatalytic Activity Evaluation

The photocatalytic activity evaluation experiments were carried out at room temperature. In each experiment, 30 mg/L TC solution was prepared as antibiotic simulated wastewater, and then 50 mL simulated wastewater was measured in a quartz glass reaction tube, in which a certain amount of photocatalyst was then added. After that, the reaction tube was placed in the photocatalytic reaction device. The process was first happened in dark with the magnetic stirring and air pumping for 30 min, so as to achieve an adsorption-desorption balance between the catalyst and the pollutants to be degraded. And then, the visible light source (45W energy-saving lamp) started irradiating. After a period of photocatalytic reaction, small amount of supernatant was sampled and taken in a quartz cuvette after centrifugal separation, and its absorbance was measured at the characteristic wavelength (357 nm) of TC using an ultraviolet-visible spectrophotometer. The removal rate of pollutants (η) was calculated according to the relationship between the degradation pollutant concentration and absorbance

$$\eta = \frac{C_0 - C_t}{C_0} \times 100\,\% = \frac{A_0 - A_t}{A_0} \times 100\,\%),$$

where $C_0(A_0)$ is the initial concentration of contaminants to be degraded (absorbance); $C_t(A_t)$ is the concentration of pollutants at the photoreaction time t (min) (absorbance).

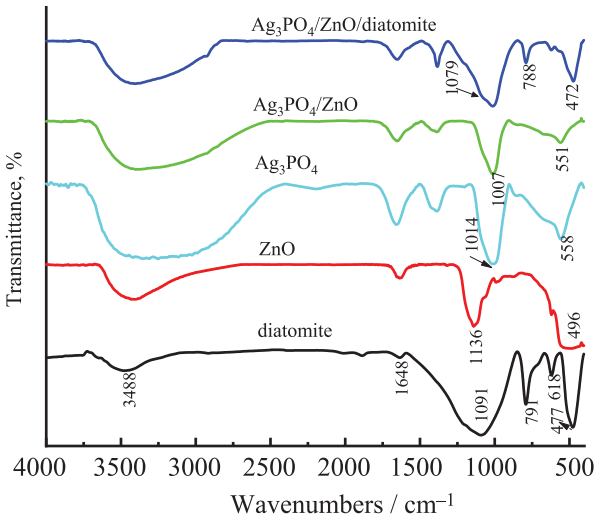

Fig. 2. (Color online) FT-IR spectra of diatomite, ZnO, Ag_3PO_4, Ag_3PO_4/ZnO and Ag_3PO_4/ZnO/diatomite.

RESULTS AND DISCUSSION

Characterization of Photocatalysts

Figure 1 shows the XRD patterns of Ag_3PO_4, ZnO, diatomite, Ag_3PO_4/ZnO and Ag_3PO_4/ZnO/diatomite. It can be seen from Fig. 1a that the characteristic diffraction peaks (JCPDS 77-1316) of the (101) and (200) crystal planes of SiO_2 appear at 2θ = 22.02° and 36.24°, respectively, in line with its main component being SiO_2. Pure Ag_3PO_4 presents a series of characteristics consistent with its body-centered cubic phase at 2θ = 20.93°, 29.74°, 33.29°, 36.67°, 47.80°, 52.77°, 55.09°, 57.32°, 61.73°and 72.05°, corresponding the crystal face of (110), (200), (210), (211), (310), (222), (320), (321), (400), and (421) respectively [11–14]. The peaks of ZnO at 2θ = 31.76°, 34.51°, 36.32°, 47.65°, 56.67°, 62.95°, and 68.01° are corresponding to (100), (002), (101), (102), (110), (103) and (112) characteristic diffraction peaks of hexagonal wurtzite [23, 35–37]. The above results indicate that Ag_3PO_4 and ZnO are body-centered cubic and hexagonal wurtzite, respectively, and the diffraction peaks of both Ag_3PO_4 and ZnO are relatively sharp, and other impurity peaks are not observed, signifying that Ag_3PO_4 and ZnO have high purity and good crystallinity. The XRD pattern of the Ag_3PO_4/ZnO composite shows that the diffraction peak of the body-centered cubic crystal type Ag_3PO_4 is still obvious, but the diffraction peak of the hexagonal wurtzite ZnO is greatly weakened due to the reduced content. Compared with pure ZnO and Ag_3PO_4, the angles of ZnO and Ag_3PO_4 in the Ag_3PO_4/ZnO composite are both slightly shifted, this shift may be caused by the formation of heterojunction during the recombination process [27]. For diatomite-introduced Ag_3PO_4/ZnO/diatomite ternary catalyst, the diffraction peaks of all the corresponding components are detected, and the diffraction peaks of the diatomite were clearer. This is because its larger particles act as a carrier and therefore it has better exposure. Compared with the Ag_3PO_4/ZnO binary catalyst, the diffraction peak of ZnO in the ternary catalyst is clearer. This may be due to the introduction of the support of diatomite, which affects the dispersibility of Ag_3PO_4 and ZnO and increases the exposed surface of ZnO crystals. In addition, as can be seen from Fig. 1b, the characteristic diffraction peak of diatomite in the ternary composite slightly shift to a low angle, which indicates that the interlayer of diatomite in the composite catalyst is slightly increased, it is possible that during the preparation of the catalyst, part of small Ag_3PO_4 particles filled some of the pore canal of the diatomite. At the same time, the diffraction peak of ZnO in the ternary catalyst shift to a high angle to some extent. This may be caused by the formation of a partial heterojunction between Ag_3PO_4 and ZnO. Interestingly, there is a weak Ag^0 diffraction peak at 2θ = 37.84°, which may be the partial reduction of Ag^+ in Ag_3PO_4, but from its intensity and position, the Ag^0 content is very low [34, 38]. The above results indicate that Ag_3PO_4/ZnO/diatomite composited successfully.

Figure 2 shows the FT-IR spectra of diatomite, ZnO, Ag_3PO_4, Ag_3PO_4/ZnO, and Ag_3PO_4/ZnO/diatomite. From this figure, the absorption peaks at 3488 and 1648 cm^{-1} are attributed to the stretching vibration and bending vibration of hydroxyl adsorbed on the surface of the catalyst [37, 39]. The absorption peaks at 1091, 791, 618, and 477 cm^{-1} correspond to the antisymmetric stretching vibration, symmetric stretching vibration, in-plane and out-plane bending vibration of the Si–O–Si bond in diatomite, respectively [34, 40]. It is confirmed that the main component of diatomite is SiO_2, which is consistent with the XRD characterization results. The strong absorption peak at 1136 cm^{-1} and the broad blunt absorption peak at 496 cm^{-1} are attributed to the symmetric stretching vibration and bending vibration absorption of the Zn–O bond of ZnO [37, 41]. The absorption peaks around 1014 and 558 cm^{-1} correspond to the stretching vibration and bending vibration of the P–O bond in Ag_3PO_4, respectively [12, 42]. Compared with pure Ag_3PO_4 and ZnO, the characteristic absorption

peak of ZnO is not clearly observed in Ag_3PO_4/ZnO binary catalyst, but both the stretching vibration and bending vibration absorption peaks of the P–O bond of Ag_3PO_4 in the binary catalyst have redshift, and the width of the absorption peak changed a little too, which may be caused by the formation of a heterojunction after the composition of Ag_3PO_4 and ZnO. Compared with the binary catalyst, the width of the stretching vibration absorption peak of P-O bond in the Ag_3PO_4/ZnO/diatomite ternary composite catalyst is widened, and also shows a Si–O–Si shoulder peak at about 1079 cm^{-1}, which is resulted from the partial overlap of the P–O bond absorption peak and the Si–O–Si bond absorption peak. In addition, compared with pure diatomite and the binary catalyst, a small red shift of the Si–O–Si bond absorption peaks and P-O bond absorption peak of the ternary composite catalyst appears, and the P–O bond bending vibration absorption of the this catalyst is basically disappeared. This may be caused by the fact that part of Ag_3PO_4 enters the pore canal of diatomite in the composite catalyst, resulting in the change of interaction between the electrons of Si–O–Si bond, which make the bond length increasing and the bond energy weakening, thereby change the position of its absorption peak. The above analysis is in accordance with the XRD characterization results.

The XPS full spectrum of Ag_3PO_4/ZnO/diatomite ternary catalyst and the high resolution XPS spectra of Ag, P, Zn, O and Si are shown in Fig. 3. According to the XPS spectrum of Ag_3PO_4/ZnO/diatomite in Fig. 3a, Ag, P, Zn, O and Si elements in the ternary catalyst were detected one by one. The characteristic peaks of Ag $3d_{3/2}$ and Ag $3d_{5/2}$ with binding energies of 373.47 and 367.45 eV in Fig. 3b and the peak of P 2p focused on 132.37 eV in Fig. 3c show that the valence of Ag element and P element in the composite catalyst is +1 and +5, respectively [12, 14, 43]. The results indicate that the valence state of Ag and P element in the catalyst does not change, but compared with the binding energies of Ag $3d_{3/2}$ (373.65 eV), Ag $3d_{5/2}$ (367.63 eV) and P 2p (132.48 eV) of pure Ag_3PO_4 reported by our research group [34], the binding energy position of Ag 3d and P 2p in the ternary catalyst shift obviously, illustrating that the electron cloud density around Ag and P elements changes to some extent in the ternary catalyst, and also electron interactions occurs among the components. As with the XRD results, a weak peak of Ag^0 was found in the spectrum, which also indicated that some Ag^0 may generated in the composite. Fig. 3d shows the XPS spectrum of Zn 2p in ternary composite. In this figure, the peaks at 1044.55 and 1021.52 eV are assigned to Zn^{2+} [44]. Figure 3e shows the O 1s spectrum of the catalyst, and the characteristic peaks of the binding energy at 531.82 and 530.22 eV correspond to the binding energy of hydroxyl oxygen adsorbed on the surface and lattice oxygen of the catalyst, respectively [14, 44]. Moreover, the relative strength of lattice oxygen peak in the catalyst is relatively high, this may be caused by the formation of heterojunction between Ag_3PO_4 and ZnO, which results in partial lattice defects, and it consistent with the results of XRD characterization. Fig. 3f is the XPS spectrum of Si 2p. It can be seen from the figure that the binding energy of Si 2p is concentrated about 102.50 eV, indicating that the valence of Si elements in the catalyst is +4, which corresponds to the Si elements in SiO_2, the main component of diatomite.

Figure 4 is the SEM images of diatomite, Ag_3PO_4, Ag_3PO_4/ZnO/diatomite and EDS spectrum of Ag_3PO_4/ZnO/diatomite. As can be seen from Figs. 4a and 4b, diatomite possesses most porous disc-shaped structure with a diameter between 10–30 μm and a few irregular block structure, while Ag_3PO_4 is mainly granular and varies in size. In the Ag_3PO_4/ZnO/diatomite ternary composite catalyst, small particles of Ag_3PO_4 are dispersed or covered on the plate-shaped ZnO surface, which can be observed from Figs. 4c–4g, especially from Fig. 4f. In addition, Ag_3PO_4 and ZnO are well dispersed on the surface and surrounding of diatomite, forming a close contact interface. The porous disc-like or block-like structure of diatomite is still clearly visible, and some Ag_3PO_4 particles are filled into the pores and the cavity of diatomite, which reduces the agglomeration between Ag_3PO_4 particles. At the same time, the surface of diatomite becomes rougher, which is conducive to the improvement of catalyst adsorption performance and the increase of photocatalytic active sites. Figure 4h is the EDS spectrum of the Ag_3PO_4/ZnO/diatomite catalyst. From this figure, it can be seen that O, Zn, Si, P and Ag elements in the catalyst are all detected, which fully corresponds to the elements composed of Ag_3PO_4/ZnO/diatomite. This result coincide with the XPS full spectrum characterization results.

Figure 5 shows TEM images of Ag_3PO_4/ZnO/diatomite ternary composite catalyst with different magnification. In Fig. 5, the structure and morphology of diatomite is not observed. Combining the results of SEM characterization, it is caused by the fact that the diameter of diatomite is too large and exceeds the detection range

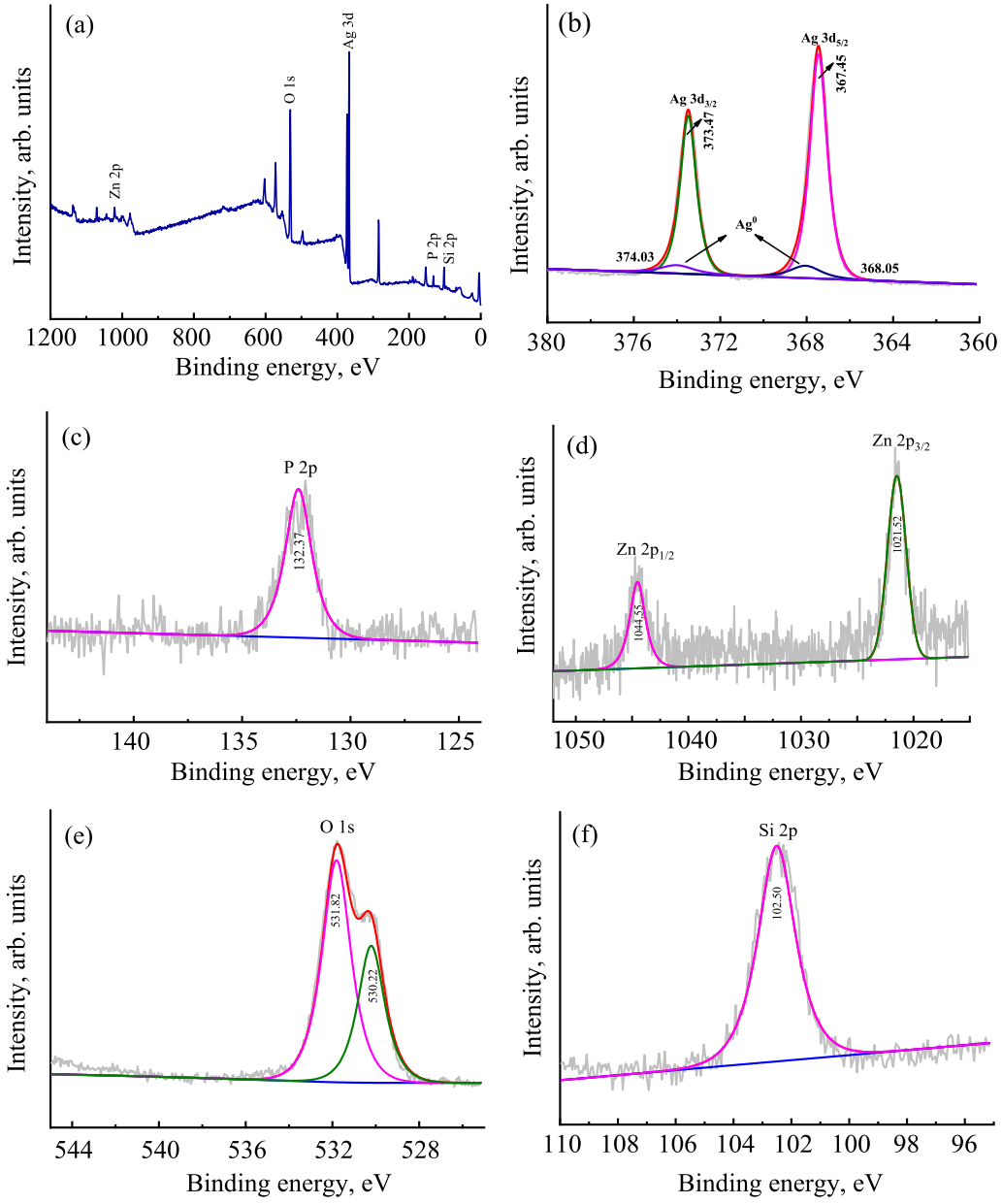

Fig. 3. XPS (a) survey spectra of the Ag_3PO_4/ZnO/diatomite composite; (b) Ag 3d; (c) P 2p; (d) Zn 2p; (e) O 1s; (f) Si 2p.

of TEM. However, the existence of Ag_3PO_4 and ZnO semiconductors can be clearly observed. The darker semiconductor is Ag_3PO_4 and the lighter semiconductor is ZnO. These two semiconductors penetrate or intimately contact to form a partial heterojunction and solid solution, and generate multiple interfaces, which is beneficial to the composite system to provide more active sites for photocatalytic reaction and faster migration and separation of photo-generated carriers. The results conform to the characterization results of XRD and FT-IR.

Figure 6 is the UV-vis DRS spectrum of Ag_3PO_4, ZnO, Ag_3PO_4/ZnO, Ag_3PO_4/ZnO/diatomite. It can be seen from Fig. 6 that Ag_3PO_4 has a certain light absorption capacity in both the ultraviolet and visible regions, while ZnO only has a strong absorption capacity for ultraviolet light, which is caused by the difference of their band gaps [11, 21]. After the combination of the two species, the absorption capacity of the catalyst in the wavelength range of 300–500 nm greatly improved compared to pure Ag_3PO_4. This can be attributed to the formation of a heterojunction in the binary

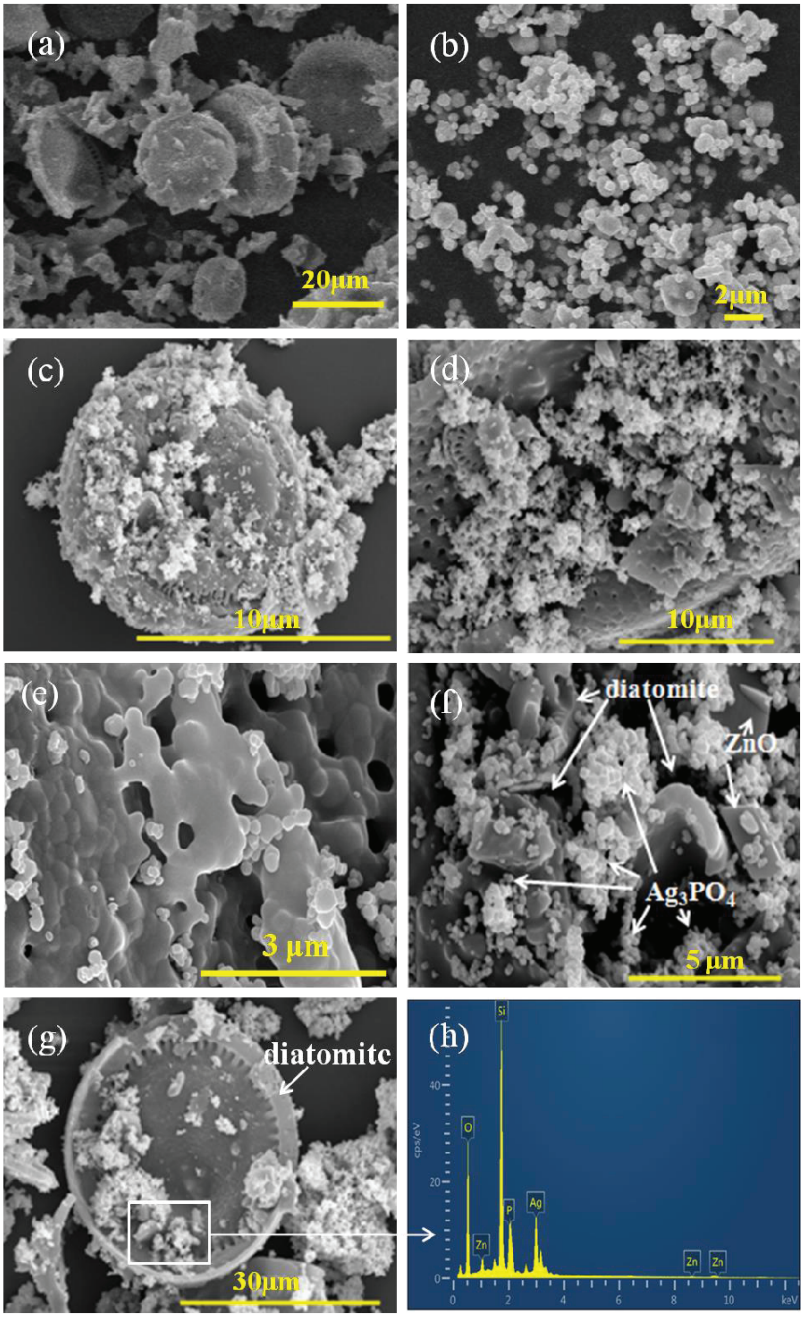

Fig. 4. SEM images of (a) diatomite, (b) Ag_3PO_4, and (c–g) Ag_3PO_4/ZnO/diatomite and (h) EDS spectrum of Ag_3PO_4/ZnO/diatomite.

catalyst. Because of the existence of heterojunction, Ag_3PO_4 can effectively transfer the photo-generated electrons, therefore, the light absorption capacity and light quantum efficiency of the catalyst are enhanced. The diatomite-loaded ternary composite catalyst has a further enhanced light absorption capacity in the visible light range and a wider spectral response range. Besides, a small amount of Ag^0 in the composite can also play a role in separating photo-generated electrons and adjusting the energy band, so that the light absorption ability of composite is enhanced [38]. According to Kubelka–Munk formula [45] and after converting and graphing (Fig. 6b), the band gap values of ZnO, Ag_3PO_4, Ag_3PO_4/ZnO and Ag_3PO_4/ZnO/diatomite catalysts are 3.14, 2.45, 2.46 and 2.28 eV, respectively. From the calculation results, it can be seen that the band gap of the

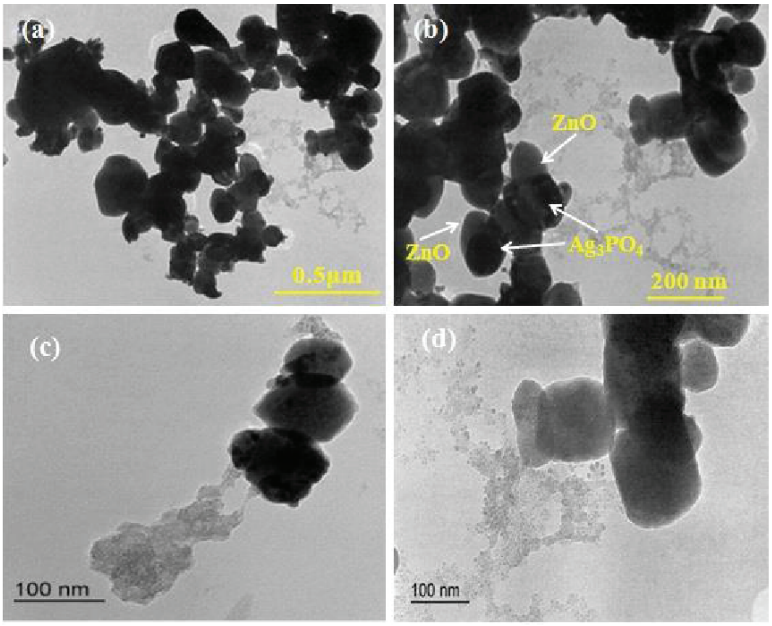

Fig. 5. TEM images of Ag_3PO_4/ZnO/diatomite photocatalyst with different magnification.

Ag_3PO_4/ZnO composite catalyst (E_g = 2.46 eV) is close to that of pure Ag_3PO_4 (E_g 2.45 eV). However, the band gap of pure ZnO is much larger than that of Ag_3PO_4, the possible reason may be that the heterojunction between them leads to a strong interface effect or quantization effect. The band gap of Ag_3PO_4/ZnO/diatomite ternary composite catalyst reduce to 2.28 eV. Combining with the SEM characterization results, this is mainly due to the effective dispersion of Ag_3PO_4 and ZnO on the surface of diatomite, and there is a strong interface effect between them. Reducing the band gap and enhance of the visible light response ability of the catalyst is beneficial to its improvement of visible light catalytic activity.

Photocatalytic Performance of Catalysts

Taking 30 mg/L TC as the degradation object without adjusting pH, diatomite, ZnO, Ag_3PO_4, Ag_3PO_4/ZnO and Ag_3PO_4/ZnO/diatomite were added respectively to the solution under visible light at the catalyst dosage of 0.4 g/L, reaction time of 120 min, and the experimental results are shown in Fig. 7. It can be seen from Fig. 7 that pure diatomite shows a certain effect on TC removal, which is because the diatomite itself has a unique pore-like structure that makes it perform well adsorption property. When pure ZnO and pure Ag_3PO_4 are used as single-component catalysts, the

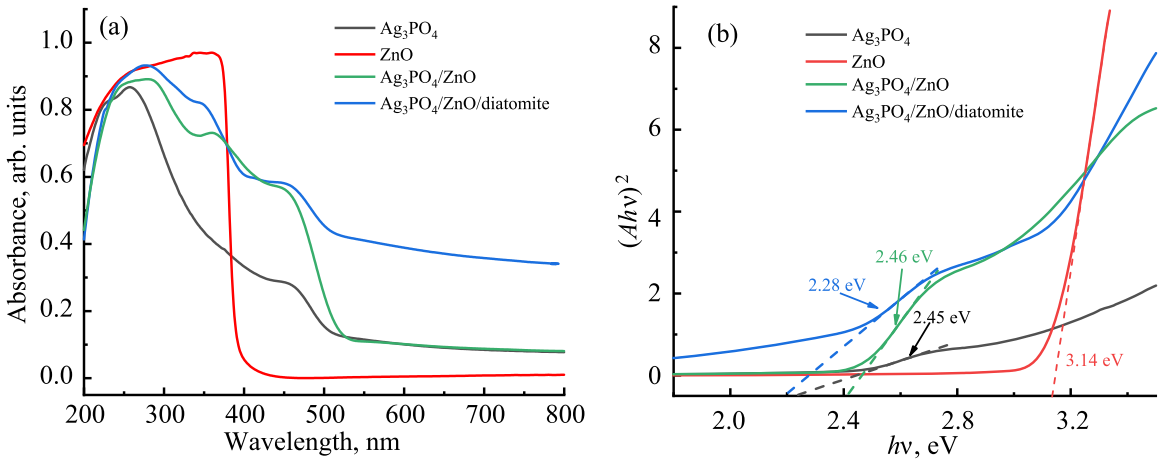

Fig. 6. (a) UV-vis DRS spectra of Ag_3PO_4, ZnO, Ag_3PO_4/ZnO and Ag_3PO_4/ZnO/diatomite and (b) plots of $(Ahν)_2$ vs. hν for Ag_3PO_4, ZnO, Ag_3PO_4/ZnO and Ag_3PO_4/ZnO/diatomite.

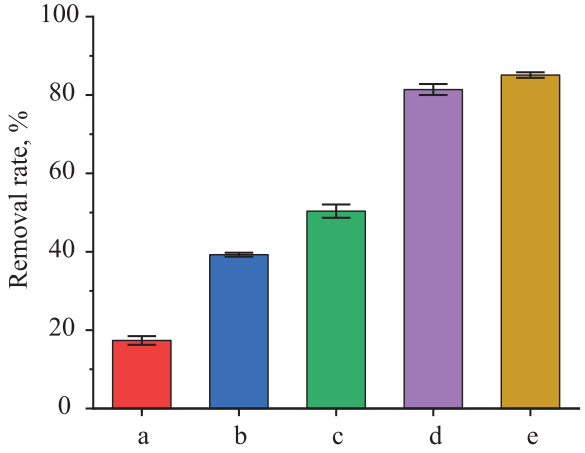

Fig. 7. The degradation of TC by (a) diatomite; (b) ZnO; (c) Ag_3PO_4; (d) Ag_3PO_4/ZnO and (e) Ag_3PO_4/ZnO/diatomite.

TC degradation effect is poor. However, the activity of the composite Ag_3PO_4/ZnO binary catalyst is significantly higher than that of the single-component catalyst. Combined with the characterization results, this may be attributed to that the recombination of the narrow band gap Ag_3PO_4 and ZnO enhance the light absorption capacity of the catalyst in the visible light region. At the same time, the heterojunction between Ag_3PO_4 and ZnO with good electron transport ability can promote the separation of photo-generated electrons and holes in Ag_3PO_4/ZnO, suppress the photocorrosion of Ag_3PO_4, and improve the photocatalytic activity of the catalyst. In addition, as can be seen from Fig. 7, the photocatalytic activity of the ternary catalyst is further improved than that of the binary catalyst. This aspect may be due to the better adsorption performance, light response ability and electron-hole separation ability of the ternary catalyst than binary catalyst. Moreover, each component in the composite system promotes the red shift of the absorption edge of the catalyst through interface effect and quantum effect, making the visible light response ability be further enhanced, and improving the photocatalytic activity.

Effects of Operational Parameters on TC Degradation

In the photocatalytic reaction, the performance of the photocatalyst is greatly affected by the reaction conditions. In order to make Ag_3PO_4/ZnO/diatomite exert the best photocatalytic performance on TC removal, the amount of catalyst dosage, initial pH value of the solution and reaction time of the photocatalytic

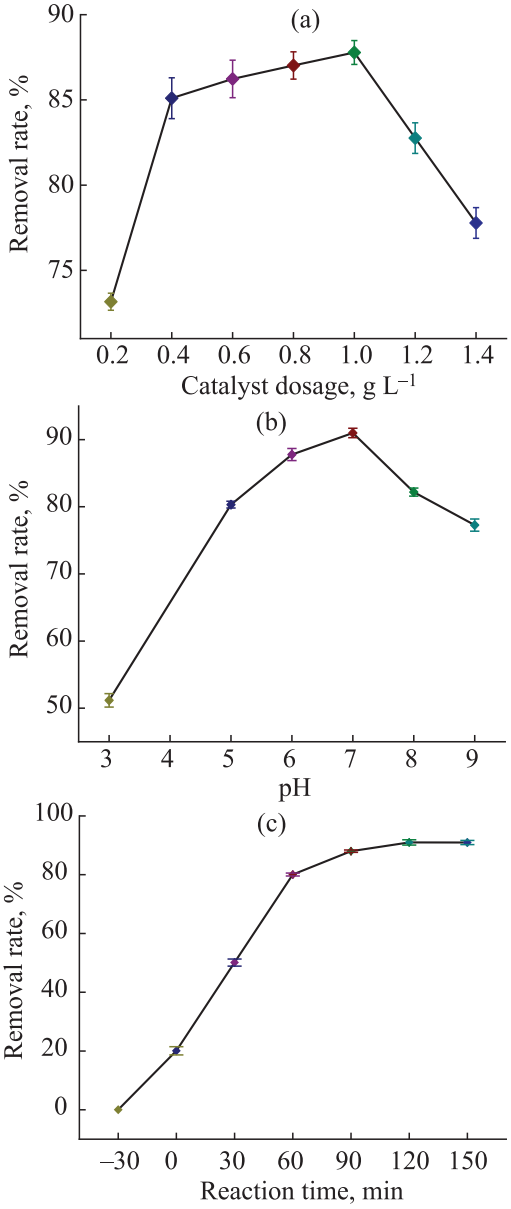

Fig. 8. The photocatalytic degradation efficiencies of Ag_3PO_4/ZnO/diatomite photocatalyst. (a) with various catalyst dosages; (b) at various initial pH of TC; (c) with various reaction times.

performance were investigated. The results are shown in Fig. 8.

Figure 8a shows the result of Ag_3PO_4/ZnO/diatomite for TC degrading under visible light with different dosages of catalyst and 120 min of the reaction time. It can be seen from Fig. 8a that the Ag_3PO_4/ZnO/diatomite has the highest removal rate when the catalyst dosage is 1.0 g/L. But when the dosage exceeds 1.0 g/L, the removal rate has actually decreased. It can be ascribed to that absorption of light by catalyst has reached its

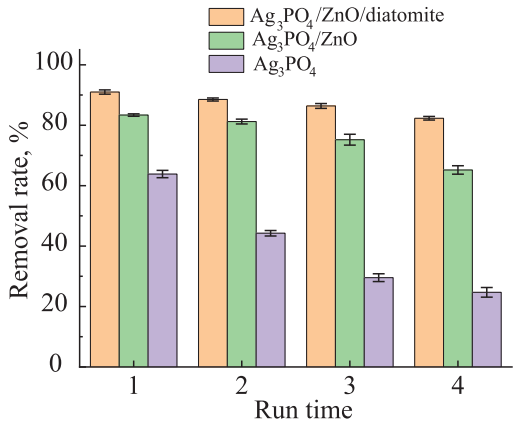

Fig. 9. Cycling runs of Ag_3PO_4/ZnO/diatomite and pure Ag_3PO_4 for the degradation of TC.

limitation when the dosage is 1.0 g/L, while the excess catalyst will cause increasing of the reaction system turbidity, as well as scattering of the light, therefore affecting of the photons absorption. In conclusion, the dosage is selected to be 1.0 g/L in the following experiment.

The effect of solution pH on the removal rate is shown in Fig. 8b.The excellent removal rate can be observed in the pH of 7. And the photocatalytic activity decreases rapidly in acidic and basic conditions. The reason for this decrease may be related to the surface charge modifications of TC and Ag_3PO_4/ZnO/diatomite catalyst at different pH values. The forms of TC existing in solution at different pH are shown in Table 1 [46]. Besides, the surface of Ag_3PO_4/ZnO/diatomite is positive charged in acidic condition and negative charged in basic condition. Therefore, the coulomb repulsion between catalyst and TC molecules is disadvantage of the adsorbing and degrading TC by catalyst, resulting in a decrease of the photocatalytic activity. Considering that the original pH of the TC solution is close to neutral (about 6), and based on the experimental results, the pH value of the following experimental TC solution is adjusted to 7.

To determine the optimal reaction time, TC degradation efficiencies of Ag_3PO_4/ZnO/diatomite was tested under the optimal dosage of the catalyst and pH value of the solution, and the result is shown in Fig. 8c. It can be seen from Fig. 8c, after 30 min dark adsorption, the removal rate reaches about 20%, this can owes to the good adsorb ability of catalyst. And the removal rate increases immediately after 60 min of exposure to light. Then, the removal rate levels off and reaches a stable value at 120 min. This could be explained by that the degradation process of TC by Ag_3PO_4/ZnO/diatomite is the process of adsorption–surface catalytic oxidation–desorption, so the reaction rate is fast at the beginning and later slow. Therefore, the best reaction time is 120 min for this system.

Table 1. The forms of TC at different pH

pH	<3.3	3.3~7.7	7.7~9.7	>9.7
TC forms	TCH_3^+	TCH_2^0	TCH^-	TC^{2-}

Reusability

The poor stability of Ag_3PO_4 catalyst is a major problem in its application. In order to investigate the stability of Ag_3PO_4/ZnO/diatomite catalyst, four consecutive degradation experiments are conducted using Ag_3PO_4/ZnO/diatomite under the above optimal reaction conditions, while Ag_3PO_4 is used as a control. After each reaction, the catalysts are centrifuged, washed with pure water and then dried, and the next degradation experiment is tested immediately. The results are shown in Fig. 9. It can be seen from Fig. 9 that the removal rate is less than 20% of pure Ag_3PO_4, while it's still above 82% of Ag_3PO_4/ZnO/diatomite after four consecutive cycles. And the stability of Ag_3PO_4/ZnO is better than pure Ag_3PO_4, but slightly worse than Ag_3PO_4/ZnO/diatomite, confirming that the stability of Ag_3PO_4/ZnO/diatomite has a significant improvement. This is because strong synergy and interfacial interaction have occurred between the components in the ternary catalyst, and the formation of heterojunction and negatively charged diatomite on the surface can promote the separation of photo-generated electrons (e^-) and holes (h^+), as well as reduce the photocorrosion of Ag_3PO_4. Hence, the activity and stability Ag_3PO_4/ZnO/diatomite catalyst are improved obviously, and it has a good practical application value.

Photocatalytic Mechanism

In order to determine the main active species of Ag_3PO_4/ZnO/diatomite in TC degradation and provide a basis for the proposition of the photocatalytic reaction mechanism, free radical trapping experiments were carried out by using EDTA-2Na, benzoquinone (BQ) and isopropanol (IPA) to capture h^+, $\bullet O_2^-$ and •OH [34, 47]. The changes of removal rate at different trapping agent are shown in Fig. 10. It can be seen from the figure that when EDTA-2Na, BQ and IPA are added to

the reaction system, the removal rate of TC decreases to varying degrees, and the decreasing order is: EDTA-2Na > BQ > IPA, indicating that h^+ and $\bullet O_2^-$ are the main active species, and •OH is the secondary active species in this reaction system.

Based on the above analysis, the possible electron transfer mechanism for Ag_3PO_4/ZnO/diatomite heterojunction system is proposed and shown in Fig. 11. In the ternary composite, since the CB and VB potentials of ZnO are more negative than those of Ag_3PO_4, it is beneficial for the formation of Ag_3PO_4/ZnO heterojunction which can uniformly dispersed on the surface of diatomite. During the photocatalytic reaction, TC is adsorbed on the catalyst surface by diatomite. At the same time, Ag_3PO_4 can be easily excited to produce e^-–h^+ pairs by its narrow bandgap under visible light irradiation, then the e^- of Ag_3PO_4 will quickly transfer to ZnO under the action of the internal electric field through the heterojunction between Ag_3PO_4 and ZnO. At this moment, the e^- transferred to ZnO can transport to the CB of ZnO under the excitation of visible light which energy is lower than the band gap of ZnO. As the previous research reported, the CB potential of ZnO (–0.35 V) is usually negative than the oxygen reduction potential ($O_2/\bullet O_2^-$: –0.33 V) [24], so e^- on the CB of ZnO can reduce the adsorbed O_2 on the catalyst surface to $\bullet O_2^-$. It is worth mentioning that in the earlier research, it was confirmed that Ag particles can also play a role in separating photogenerated electrons to generate $\bullet O_2^-$, which may also be a secondary factor in this system [34, 38]. Furthermore, $\bullet O_2^-$ can further oxidize and decompose TC to H_2O, CO_2 and small molecule inorganic salt. Besides, due to the more positive VB potential of Ag_3PO_4, the h^+ on its VB has strong oxidizing ability, which can also oxidize and decompose TC. In addition, diatomite, as a typical silicate, is rich of negative charge on its surface, which can effectively separate the positively charged h^+ and negatively charged e^- in Ag_3PO_4 by charge attraction and repulsion. The rapid e^-–h^+ separation and transfer and the electrostatic effect of diatomite may avoid the photocorrosion of Ag_3PO_4, reduce the recombination probability of e^- and h^+, and improve the photocatalytic activity and stability of Ag_3PO_4/ZnO/diatomite.

CONCLUSIONS

In summary, Ag_3PO_4/ZnO/diatomite composite photocatalyst was successfully prepared by ultrasonic dispersion-precipitation method. The characterization results show that the heterojunctions, formed between Ag_3PO_4 and ZnO, was well dispersed on the surface of diatomite. What's more, there are also a few small Ag_3PO_4 particles filled the pores of diatomite. The interactions among the components in the catalyst have improved the adsorption performance of the catalyst, the light absorption capacity and the separation ability of photo-generated e^- and h^+, which makes the Ag_3PO_4/ZnO/diatomite ternary composite photocatalyst exhibit better photocatalytic activity than the monomer photocatalysts and Ag_3PO_4/ZnO binary photocatalysts. When the dosage of catalyst was 1.0 g/L, the initial pH of the solution was 7 and the reaction was conducted under

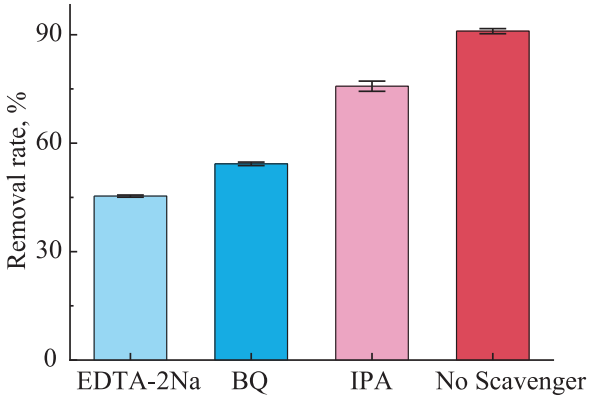

Fig. 10. Photocatalytic efficiency of the Ag_3PO_4/ZnO/diatomite composite for the degradation of TC with the addition of different scavengers.

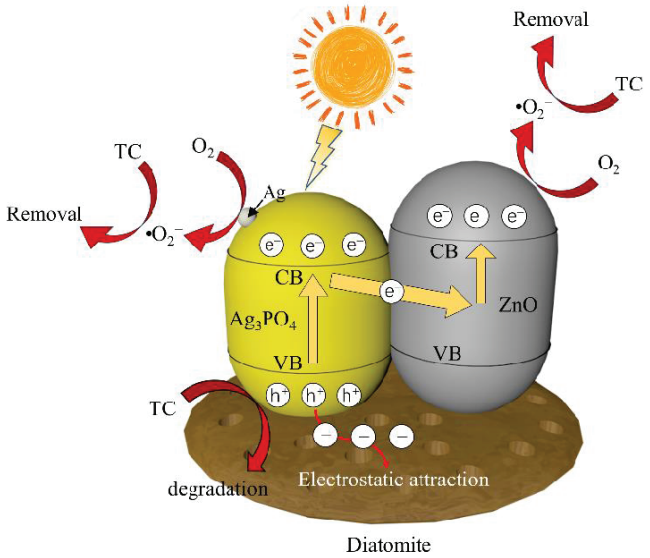

Fig. 11. The proposed photocatalytic mechanism of Ag_3PO_4/ZnO/diatomite composite.

visible light for 120 min, the removal rate of 30 mg/L TC by Ag_3PO_4/ZnO/diatomite photocatalyst was up to 90.99%. At the same time, the heterojunction formed between Ag_3PO_4 and ZnO and the electrostatic effect of the negative charge on the surface of diatomite make the e^- on the surface of Ag_3PO_4 transfer quickly, which effectively inhibits the photocorrosion of e^- to Ag_3PO_4 and makes the catalyst exhibit good stability. After the photocatalyst was used for 4 times continuously under the same reaction conditions as above, the TC removal rate of the ternary composite photocatalyst remained above 82%. This study proves that the Ag_3PO_4/ZnO/diatomite photocatalyst is a promising visible-light photocatalyst for TC waste water treatment.

ACKNOWLEDGMENTS

We gratefully acknowledge the financial supports from the National Natural Science Foundation of China (no. 51974267) Sichuan science and technology support project (2020JDTD0018) and the Foundation of Youth Science and Technology Innovation Team of Sichuan Province (grant no. 2015TD0007).

CONFLICT OF INTEREST

The authors declare that they have no conflict of interest.

REFERENCES

1. Kümmerer, K., *Chemosphere*, 2009, vol. 75, no. 4, pp. 417–434. https://doi.org/10.1016/j.chemosphere.2008.11.086
2. Bu, Q.W., Wang, B., Huang, J., et al., *Chemosphere*, 2016, vol. 144, pp. 1384–1390. https://10.1016/j.chemosphere.2015.10.010
3. Gupta, P.V., Nirwane, A M., Bellubi, T., et al., *Nanomedicine*, 2017, vol. 13, no. 7, pp. 2371–2384. https://doi.org/10.1016/j.nano.2017.06.011
4. Zhang, Q., Ying, G., Pan, C., et al., *Environ. Sci. Technol*., 2015, vol. 49, no. 11, pp. 6772–6782. https://doi.org/10.1021/acs.est.5b00729
5. Nghiem, L D., Manis, A., Soldenhoff, K., et al., *J. Membrane Sci*., 2004, vol. 242, no. 1-2, pp. 37–45. https://doi.org/10.1016/j.memsci.2003.12.034
6. Ternes, T A., Stueber, J., Herrmann, N., et al., *Water Res*., 2003, vol. 37, no. 8, pp. 1976–1982. https://doi.org/10.1016/S0043-1354(02)00570-5
7. Huber, M.M., Canonica, S., Park, G.Y., et al., *Environ. Sci. Technol*., 2003, vol. 37, no. 5, pp. 1016–1024. https://doi.org/10.1021/es025896h
8. Ma, S., Gu, J., Han, Y., et al., *ACS Omega*, 2019, vol. 4, no. 25, pp. 21063–21071. https://doi:10.1021/acsomega.9b02411
9. Jiao, S., Zheng, S., Yin, D., et al., *Chemosphere*, 2008, vol. 73, no. 3, pp. 377–382. https://doi.org/10.1016/j.chemosphere.2008.05.042
10. Zhu, P., Ren, Z., Wang, R., *Front. Mater. Sci.*, 2020, vol. 14, no. 1, pp. 33–42. https://doi.org/10.1007/s11706-020-0486-8
11. Yi, Z., Ye, J., Kikugawa, N., et al., *Nat. Mater*., 2010, vol. 9, no. 7, pp. 559–564. https://doi.org/10.1038/nmat2780
12. Chen, Y., Zhu, P., Duan, M., et al., *Appl. Surf. Sci*., 2019, vol. 486, pp. 198–211. https://doi.org/10.1016/j.apsusc.2019.04.232
13. Bi, Y., Ouyang, S., Umezawa, N., et al., *J. Am. Chem. Soc*., 2011, vol. 133, no. 17, pp. 6490–6492. https://doi.org/10.1021/ja2002132
14. Zhu, P., Chen, Y., Duan, M., et al., *Catal. Sci. Technol*., 2018, vol. 8, no. 15, pp. 3818–3832. https://doi.org/10.1039/C8CY01087K
15. Tian, L., Yang, X., Cui, X., et al., *Appl. Surf. Sci*., 2019, vol. 463, pp. 9–17. https://doi.org/10.1016/j.apsusc.2018.08.209
16. Kim, Y.G. and Jo, W.K., *J. Hazard. Mater*., 2019, vol. 361, pp. 64–72. https://doi.org/10.1016/j.jhazmat.2018.08.074
17. Zhang, H.S., Yu, D., Wang, W., et al., *Advanced Powder Technol*., 2019, vol. 30, no. 9, pp. 1910–1919. https://doi.org/10.1016/j.apt.2019.06.010
18. Teng, W., Tan, X., Li, X., et al., *Appl. Surf. Sci*., 2017, vol. 409, pp. 250–260. https://doi.org/10.1016/j.apsusc.2017.03.025
19. Shi, W.L., Liu, C., Li, M.Y., et al., *J. Hazard. Mater.*, 2020, vol. 389, pp. 121907. https://doi.org/10.1016/j.jhazmat.2019.121907
20. Tang, M.L., Ao, Y.H., Wang, C., et al., *Appl. Catal. B*., 2020, vol. 268, pp. 118395. https://doi.org/10.1016/j.apcatb.2019.118395
21. Ong, C.B., Ng, L.Y., and Mohammad, A.W., *Renew. Sust. Energ. Rev*., 2018, vol. 81, pp. 536–551. https://doi.org/10.1016/j.rser.2017.08.020
22. Qi, K.Z., Cheng, B., Yu, J.G., et al., *J. Alloys Compd.*, 2017, vol. 727, pp. 792–820. https://doi.org/10.1016/j.jallcom.2017.08.142
23. Qu, Y.N., Xu, X.J., Huang, R.L., et al., *Chem. Eng. J*., 2020, vol. 382, pp. 123016. https://doi.org/10.1016/j.cej.2019.123016

24. Ruan, S.H., Huang, W.Q., Zhao, M.J., et al., *Mater. Sci. Semicond. Process*., 2020, vol. 107, pp. 104835. https://doi.org/10.1016/j.mssp.2019.104835
25. Fernández, L., Gamallo, M., González-Gómez, M.A., et al., *J. Environ. Manag*., 2019, vol. 237, pp. 595–608. https://doi.org/10.1016/j.jenvman.2019.02.089
26. Li, Q. and Yang, C., *Mater. Lett*., 2017, vol. 199, pp. 168–171. https://doi.org/10.1016/j.matlet.2017.04.058
27. Martin-Gomez, A., Navio, J., Jaramillo-Paez, C., et al., *J. Photoch. Photobio. A*., 2020, vol. 388, pp. 112196. https://doi.org/10.1016/j.jphotochem.2019.112196
28. Wu, Q., Wang, P., Niu, F., et al., *Appl. Surf. Sci*., 2016, vol. 378, pp. 552–563. https://doi.org/10.1016/j.apsusc.2016.03.158
29. Sharma, M., Ojha, K., Ganguly, A., et al., *New J. Chem*., 2015, vol. 39, no. 12, pp. 9242–9248. https://doi.org/10.1039/C5NJ01157D
30. Chai, Y., Ding, J., Wang, L., et al., *Appl. Catal. B*., 2015, vol. 179, pp. 29–36. https://doi.org/10.1016/j.apcatb.2015.05.006
31. Luo, J., Duan, G., Wang, W., et al., *Appl. Clay Sci*., 2017, vol. 143, pp. 273–278. https://doi.org/10.1016/j.clay.2017.04.004
32. Ma, J., Liu, Q., Zhu, L., et al., *Appl. Catal. B*., 2016, vol. 182, pp. 26–32. https://doi.org/10.1016/j.apcatb.2015.09.004
33. Ma, J., Zou, J., Li, L., et al., *Appl. Catal. B*., 2014, vol. 144, pp. 36–40. https://doi.org/10.1016/j.apcatb.2013.06.029
34. Zhu, P., Chen, Y., Duan, M., et al., *Powder Technol*., 2018, vol. 336, pp. 230–239. https://doi.org/10.1016/j.powtec.2018.05.060
35. Tadjarodi, A., Izadi, M., Imani, M., *Mater. Lett*., 2013, vol. 92, pp. 108–110. https://doi.org/10.1016/j.matlet.2012.10.045
36. Shaker-Agjekandy, S., Habibi-Yangjeh, A., *Mater. Sci. Semicond. Process*., 2015, vol. 34, pp. 74–81. https://doi.org/10.1016/j.mssp.2015.02.022
37. Zhu, P., Chen, Y., Duan, M., et al., *Russ. J. Appl. Chem*., 2016, vol. 89, no. 12, pp. 2027−2034. https://doi.org/10.1134/S1070427216120144
38. Fan, H., Ren, Q., Wang, S., Jin, Z., Ding, Y., *J. Alloys Compd*., 2019, vol. 775, pp. 845–852. https://doi.org/10.1016/j.jallcom.2018.10.152
39. Faisal, M., Ismail, A., Ibrahim, A., et al., *Chem. Eng. J*., 2013, vol. 229, pp. 225–233. https://doi.org/10.1016/j.cej.2013.06.004
40. Liu, M., Guo, Y., Lan, J., et al., *Chemistry Select*, 2019, vol. 4, no. 45, pp. 13156–13162. https://doi.org/10.1002/slct.201903312
41. Pudukudy, M., Hetieqa, A., and Yaakob, Z., *Appl. Surf. Sci*., 2014, vol. 319, pp. 221–229. https://doi.org/10.1016/j.apsusc.2014.07.050
42. Liu, L., Ding, L., Liu, Y., et al., *Appl. Catal. B*., 2017, vol. 201, pp. 92–104. https://doi.org/10.1016/j.apcatb.2016.08.005
43. Ren, J., Chai,Y., Liu, Q., et al., *Appl. Surf. Sci*., 2017, vol. 403, pp. 177–186. https://doi.org/10.1016/j.apsusc.2017.01.172
44. Chen, S., Liu, F., Xu, M., et al., *J. Colloid Interface Sci*., 2019, vol. 553, pp. 613–621. https://doi.org/10.1016/j.jcis.2019.06.053
45. Xu, H., Wang, C., Song, Y., et al., *Chem. Eng. J*., 2014, vol. 241, pp. 35–42. https://doi.org/10.1016/j.cej.2013.11.065
46. Chang, P., Li, Z., Jean, J., et al., *Appl. Clay Sci*., 2012, vol. 67–68, pp. 158–163. https://doi.org/10.1016/j.clay.2011.11.004
47. Cao, W., Gui, Z., Chen, L., et al., *Appl. Catal. B*., 2017, vol. 200, pp. 681–689. https://doi.org/10.1016/j.apcatb.2016.07.030